Active damping of grid-connected converters with LCL filter

Comparison of common methods and further development

Mikkel Rindholt

Energy Technology, OES10-2-F19

Master Thesis

STUDENT REPORT

AALBORG UNIVERSITY

In compilation of this report, LaTeX is used as writing program. The same program has been used for constructing tables in the report. Graphs are constructed using MATLAB and simulations are created in Simulink. All pictures taken of the internet, have the appropriate citing.

Institute of Energy Technology
Aalborg University Esbjerg
www.et.aau.dk

AALBORG UNIVERSITY
STUDENT REPORT

Title:
Active damping of grid-connected converters with LCL filter

Theme:
Power Electronic Systems

Project Period:
Spring Semester 2019

Project Group:
OES10-2-F19

Participant(s):
Mikkel Rindholt

Supervisor(s):
Amin Hajizadeh

Copies: 1

Page Numbers: 79

Date of Completion:
May 30, 2019

Abstract:

For a Voltage Source Inverter (VSI), an LCL filter is one of the preferred filter methods for obtaining a close to pure sinusoidal output. Even though the LCL filter itself generate harmonic distortion in the output, many methods have been investigated to counteract this distortion. The method of using a damping resister in series with the LCL filter capacitor has proven effective, but at the cost of a significant amount of power losses. In this project three active damping methods, PR control, Notch filter and Virtual Resistor, are studied, and the Virtual Resistor chosen to replace the damping resistor. A PI controller and the Virtual Resistor is designed and tested, both through simulations and lab. testing, and the LCL filter model is subsequently validated. Meanwhile the concept of Adaptive Virtual Resistance is also explored, and a algorithm for Minimal Distortion Tracking is developed and tested through simulations.

Contents

Preface

This project is a continuation of the work, described in the project "Power Control of Grid Connected Converter for Offshore Wind Power System". The project was done in collaboration with Hisham Hasan Taleb and Waqas Aslam Cheema. A copy of the the project can be found in the appendix.

Aalborg University Esbjerg, May 30, 2019

Mikkel Rindholt
<mrindh14@student.aau.dk>

Chapter 1

Introduction

Most renewable energy producing devices, like wind turbines and solar panels, produce a DC voltage, or AC voltage which is then rectified. To connect those devices to the grid, an inverter is needed to convert the voltage into AC, which is synchronized with the grid voltage. The inverter output is not a pure sine wave but a modulated square wave, which requires a filter, for the output to resemble a sine wave. One commonly used filter is the LCL filter. This filter is effective at filtering the modulated square wave, but due to the inductor-capacitor configuration, the filter also induces harmonic distortion to the output sine wave. This has previously been connecting a damping resistor in series with the filter capacitor, to reduce that distortion. This method is effective, but results in a power loss in the resister, which both reduce the effectiveness of the DC to AC conversion, but also requires additional cooling, to remove the heat, generated by the damping resistor.

This chapter will briefly describe the above mentioned terms; inverter, LCL filter, harmonic distortion and damping resistor.

1.1 Inverter

A 2-level inverter consists of 6 IGBTs in a configuration shown on figure 1.1. The 6 IGBT pairs are controlled by a high frequency Pulse Width Modulation (PWM) signal, which is supplied by a controller. IGBTs are used for high power converters due to their high switching frequency and power handling capabilities.

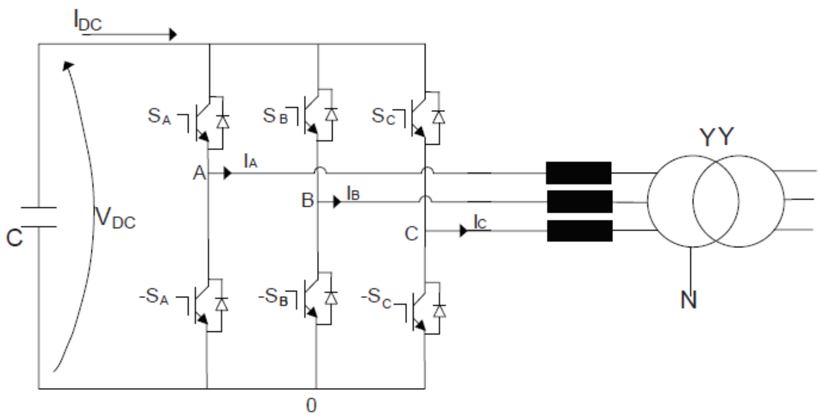

Figure 1.1: Circuit diagram of an inverter with IGBTs. [15]

Pulse Width Modulation converts a fuzzy logic control signal into a binary signal, which controls the switching of IGBT pairs. As the name suggests, the inverter controls the voltage through the width of pulses in the pulsating voltage output. Figure 1.2 shows the PWM output compared to the control input. When the PWM output is 1, the positive IGBT switch is on, and the negative IGBT switch is off. When the PWM output is -1, the negative IGBT switch is on.

The PWM signal is created by comparing a triangular signal, $Vtrig$, shown on figure 1.3, to the reference signal from the controller, $Vcontrol$. When the control signal is greater than the triangular signal, the PWM output is 1, and otherwise it is -1.

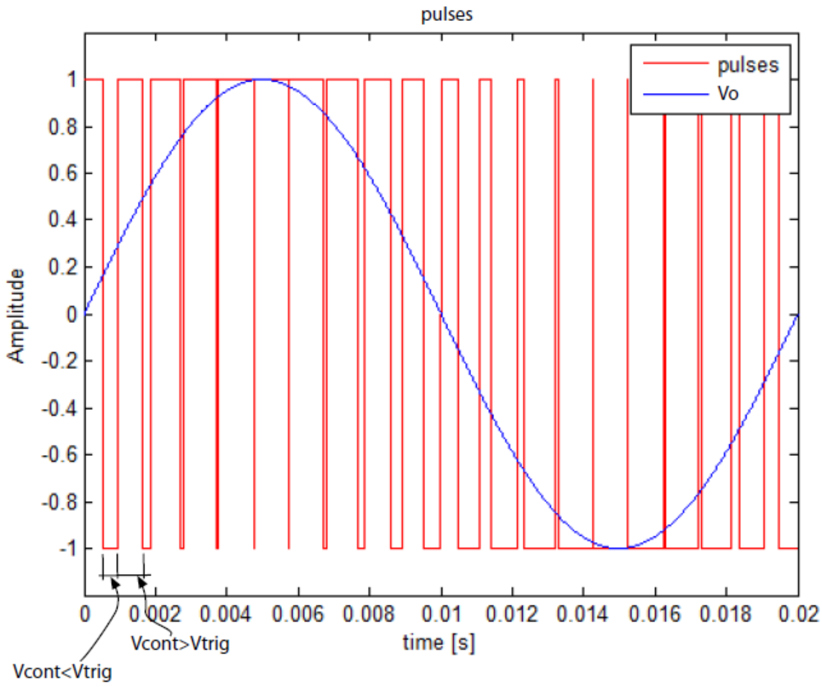

Figure 1.2: The modulated signal, controlling the IGBTs, compared to the reference signal. [15]

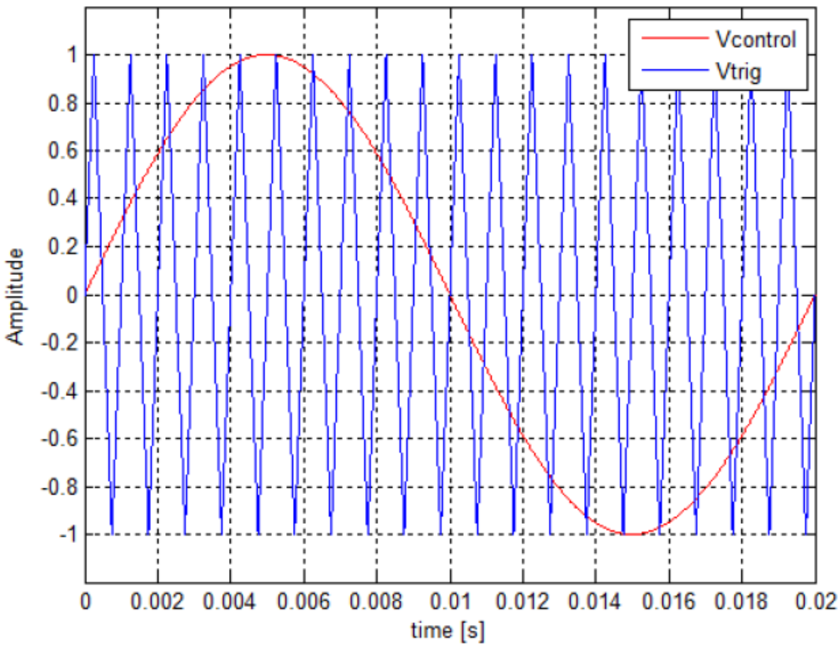

Figure 1.3: The carrier signal compared to the reference signal. [15]

1.2 LCL filter

An LCL filter consists of two inductors connected in series, with a ground connected capasitor inbetween, as shown on figure 1.4. The purpose of the LCL filter is to filter the inverter output, as that consists of a series of square waves with varying widths. Ideally, the LCL filter should filter the inverter output, so it resembles a sine wave, but the filter resonates at a specific frequency, and induces resonant distortion at that frequency. The resonance frequency depends on the characteristics of the filter. [11] [1]

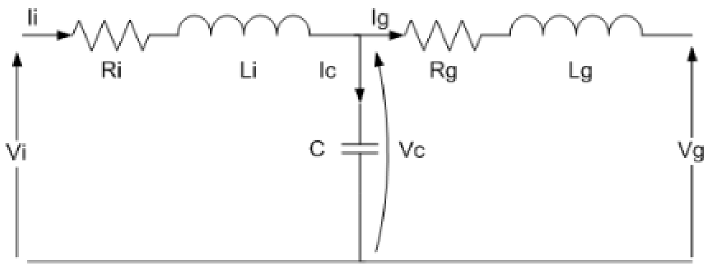

Figure 1.4: Circuit diagram of one of the phases of the LCL filter. [15]

The resonance frequency of the LCL filter, ω_r, can be calculated using equation 1.1.

$$\omega_r = \sqrt{\frac{L_i + L_g}{C L_i L_g}} \quad (1.1)$$

1.3 Damping Resistor

To combat the harmonic distortion, described in section 1.2, a damping resistor can be implemented into the filter, as shown on figure 1.5.

The resistor dampens the amplitude of the resonating current, and thereby dampens the overall resonance of the filter. As the damping resistor consumes power in the process, the overall efficiency of the inverter is decreased. Therefore a small resistance is desirable to minimize the losses, but the resistor must be large enough to provide sufficient damping. The optimal damping resistance can be calculated using 1.2.

$$R_d = \frac{1}{(3\omega_r C)} \quad (1.2)$$

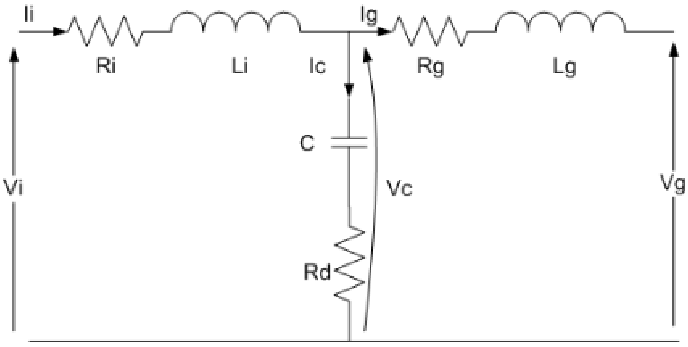

Figure 1.5: Circuit diagram of one of the phases of the LCL filter with a damping resistor. [15]

1.4 Grid standards

Many national and international standards define the rules for grid-connected inverters. This section will compare the standards for electrical characteristics of photovoltaic grid-connected inverter systems, defined by the standards for the European Union (IEC 61727:2004) and the United States (IEEE 1547:2018), in regards to harmonic current distortion.

Table 1.1: Comparison of the IEC and IEEE standards for harmonic current distortion. [13] [8]

	IEC 61727:2004	IEEE 1547:2018
Odd Harmonics	Threshold in %	Threshold in %
$\leq 9^{th}$	< 4.0	≤ 4.0
11^{th} to 17^{th}	< 2.0	≤ 2.0
17^{th} to 23^{th}	< 1.5	≤ 1.5
23^{th} to 35^{th}	< 0.6	≤ 0.6
35^{th} to 50^{th}	-	≤ 0.3
Even Harmonics	Threshold in %	Threshold in %
2^{th}	< 1.0	≤ 1.0
4^{th}		≤ 2.0
6^{th}		≤ 3.0
8^{th}		≤ 4.0
10^{th} to 14^{th}	< 0.5	≤ 2.0
16^{th} to 20^{th}	< 0.5	≤ 1.5
22^{th} to 34^{th}	< 0.5	≤ 0.6
36^{th} to 50^{th}	-	≤ 0.3
Total Rated Distortion	< 5.0	≤ 5.0

These two standards have similar requirements for the odd harmonics, but the updated IEEE 1547 have changed requirements for the even harmonics. [5]

In the latest version of the IEEE 1547 standard, the term current THD has been replaced with Total Rated Distortion (TRD), where inter-harmonic distortion is included into the total distortion calculations as well. Inter-harmonic distortion is distortion from frequencies, which are not harmonic components of the fundamental frequency. These changes might be included in a future, amended version of the IEC 61727 standard as well, as the current version will expire in 2022. [13]
For this project the results will be compared with the 5% limit for current THD, described in the IEC 61727:2004 standard.

Chapter 2

Literature review

This literature review will investigate scientific papers regarding active damping of harmonic distortion induced in an LCL filter, as described in chapter 1. The review will focus on papers describing different active control methods for reducing this type of distortion. Three active control methods have been selected for the review. These methods are PR-controller, Notch filter and Virtual Resister.

Improved passive filters methods, to reduce the power losses several different solutions have also been investigated, e.g. different configurations of resistors, inductors and capacitors to minimize the losses while still obtaining the same damping effect. [20] [18]

The common result of these solutions is reduced losses, while still maintaining an effective reduction of the distortion. However, contrary to the active damping methods, these methods do still result in losses, which is one of the key problems, that should be eliminated. Therefore, these methods will not be investigated further in this report.

2.1 PR control method

The Proportional-Resonant control method is similar to a PID controller. A PR controller is utilizing the same proportional control method, but instead of an integral and derivative component, is has a resonant component that filter resonance at a specific frequency. The controller is, like the PID controller, tuned by changing the K_p and K_r, but the harmonic resonance frequency, ω_r, is also needed to design this controller. [2]

$$G_{PR}(s) = K_p + \frac{K_r\, s}{s^2 + {\omega_r}^2} \tag{2.1}$$

The PR controller transfer-function 2.1 is the ideal controller, which filter out any noise at the specified resonance frequency. It will, however, result in an infinite gain at the resonant frequency, which should be avoided due to system instability. [16]

$$G_{PR}(s) = K_p + \frac{K_r\, \omega_c\, s}{s^2 + {\omega_c}^2 s + \omega_r} \tag{2.2}$$

In the non-ideal PR controller transfer-function 2.2, a cutoff frequency ω_c is introduced to control the bandwidth of the controller. [17]

This controller works on a stationary reference frame, meaning no phase angle detection is required. In some controller layouts, where one or more reference inputs are in a rotating reference frame, this will still be necessary for conversion into a stationary reference frame.

It is possible to improve the performance of this controller by adding filters in parallel to filter out specific lower-order harmonic frequencies as shown in figure 1. This is called Harmonic Compensation.

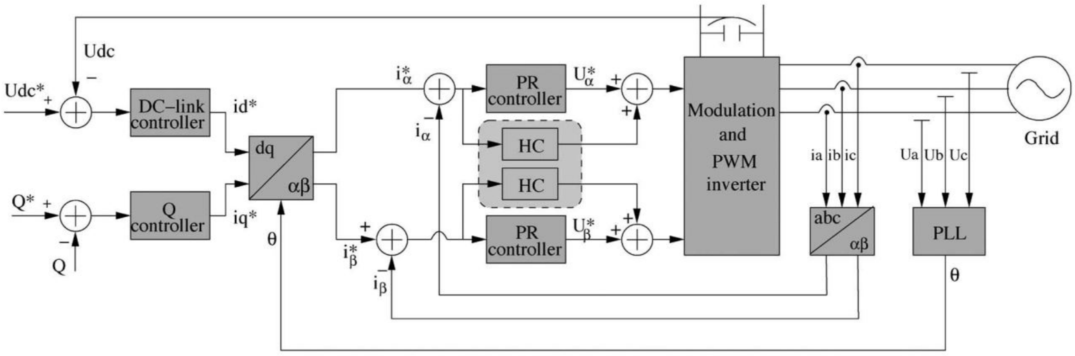

Figure 2.1: A general structure of the PR control strategy. [2]

The PR controller strategy is effective at filtering the designed resonance frequency, but in dynamic systems and setups, where external factors, like an unstable grid, change the operational conditions of the inverter, these changes could also affect the resonance frequency. Such changes could lower or even eliminate the PR controllers ability to filter out the harmonic resonance, as the frequency, the controller is designed for, does no longer match the resonance frequency of the LCL filter. However, for a non-ideal PR controller, a wider bandwidth, ω_c, can reduce the sensitivity towards small variations in the resonance frequency. [17]

2.2 Notch filter method

A Notch filter is a common filter method for filtering specific frequencies. When used to filter harmonic resonance from the LCL filter, the Notch filter is placed at the controller output, so the resonance compensation is added to the controller output. The controller could e.g. be a PI controller design. [4] [6]

A notch filter is a second order transfer function, as shown in equation 2.3, where ω_r is the resonance frequency and ζ is a damping factor, designed to get optimal damping from the notch filter.

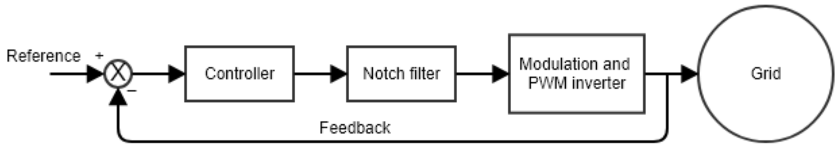

Figure 2.2: A block diagram of the notch filter method

$$G_{notch}(s) = \frac{s^2 + {\omega_r}^2}{s^2 + 2\zeta\,\omega_r\,s + {\omega_r}^2} \tag{2.3}$$

The notch filter, like the PR controller, is designed to filter out any resonant distortion at one specific frequency, so any changes to the operational conditions could change the resonance frequency of the LCL-filter and therefore make the Notch filter unable to filter out the distortion.

Another approach is to control the notch filter performance through a quality factor, q, as shown in equation 2.4. [19]

$$G_{notch}(s) = \frac{s^2 + {\omega_r}^2}{s^2 + \frac{1}{q}\,\omega_r\,s + {\omega_r}^2} \tag{2.4}$$

This approach, however, does not fundamentally change the Notch filter transfer-function, as the equations 2.3 and 2.4 only have different approaches to controlling the damping behavior of the Notch filter.

A problem for notch filters is, that the filter transfer function cannot be discretized, while maintaining the desired damping frequency. The sampling frequency and discretization method affect the center frequency of the discretized notch filter, and a discrete notch filter has another design process than the continuous filter. [6]

A solution to this problem could be to design the Notch filter in a discrete from, as shown in equation 2.5. [3]

$$G_{NF}(z) = \frac{1}{2}\left[1 + \frac{k_2 + k_1(1+k_2)z^{-1} + z^{-2})}{1 + k_1(1+k_2)z^{-1} + k_2 z^{-2}}\right] \tag{2.5}$$

The constants k_1 and k_2 of discrete Notch filter can be calculated based on the inverter switching time, T_{sw}, the resonance frequency, f_r, and the desired bandwidth of the Notch filter, B_{NF}. These can also be changed in real-time, to compensate for changes of the resonance frequency, caused by external factors.

$$k_1 = -cos(T_{sw} \cdot 2\pi \cdot f_r) \;\; and \;\; k_2 = \frac{1 - tan(T_{sw} \cdot 2\pi \cdot B_{NF}/2)}{1 + tan(T_{sw} \cdot 2\pi \cdot B_{NF}/2)} \tag{2.6}$$

The Notch filter method is effective at compensating for the resonance, also when the frequency is changing. A downside of the Notch filter is that it does compensate for other harmonic frequencies, unlike the PR control method.

2.3 Virtual Resistor method

A virtual resister is a state estimator, that estimate the voltage drop over a damping resister based on voltage or current measurements of from the LCL filter, should the resistor be present in the filter. As the damping resistor is not present, neither will the power losses, affiliated with a real damping resistor.

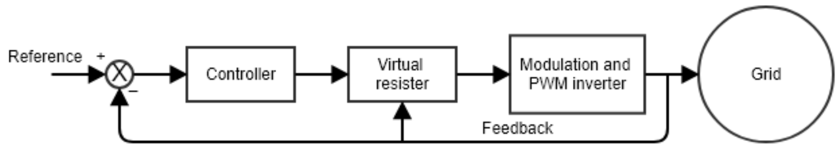

Figure 2.3: A block diagram of the virtual resistor method

Capacitor current feedback is a simple approach to create a Virtual Resistance compensator. A measurement of the capacitor current is multiplied with the desired resistance, and the resulting signal is subtracted from the control signal. [20]

Variations in this approach includes replacing the resistance multiplication operation with different types of transfer-functions, in order to obtain even better filter performance. Some of these transfer-function approaches include a second-order derivative, which, under real conditions, is difficult to achieve due to measurement noise. [10] These different approaches, that require sensors to be implemented into the LCL filter, which is not desirable, as it would add to the cost and complexity of the inverter system.

As another approach aims to utilize already existing measurement data, in order to estimate the behavior of the virtual resistor, this approach is defined as "sensorless", as it requires no additional sensors to be implemented. This approach is estimating the capacitor phase current, based on the current output of the inverter, i_a, and the estimated output of the inverter, $V_{amp} \cdot v_a^*$, where V_{amp} is the amplitude of the rated phase voltage, and v_a^* is the fundamental reference wave for the PWM. [9]

$$i_{Cfa}^* = p\, C_f(V_{amp} \cdot v_a^* - L_i\, p\, i_a) \tag{2.7}$$

The differential in this equation is represented by p.

As with the PR controller ands Notch filter methods, grid disturbances could affect the performance of the Virtual Resistor. One method attempts to address this matter by detecting grid impedance variation, and based on that adapt the Virtual Resistance to optimize the damping performance. [7]

Unlike the PR controller ands Notch filter methods, the Virtual Resistance method does not depend on a specific resonance frequency, but rather the currents, running inside the LCL filter, which can be estimated without the need for additional sensors. The Virtual Resistance method seems less effective at filtering out the specific resonance frequency, but overall more effective at filtering general distortion.

2.4 Conclusion

Many methods exist to eliminate the harmonic resonance from the LCL filter.

While the PR controller and Notch filter are effective at filtering out resonance from specific resonance frequencies, they lack the robustness of the damping resistor. The Virtual Resistance method approaches the problem from a different angle, by imitating the behavior of the damping resistor, and thereby obtaining a similar robustness as the damping resistor. However, the Virtual Resistor does not have the same filtering performance at the specific resonance frequencies, but it has an overall advantage, as it can filter many different harmonic frequencies with a single filter.

As the goal of this project is to find a robust solution to the resonance problem, the Virtual Resistance method is chosen, as it seems to provide sufficient robustness over the two other methods.

Chapter 3

Modeling and design

3.1 Equation based model

This model is based on a reference model described in the project "Power Control of Grid Connected Converter for Offshore Wind Power System"[15]. Several improvements have been made to parts of the model, and will be described in this chapter, but the general aspects of the model remain the same, and this will be noted in the specific descriptions.

Inverter model

This inverter model, unlike in the reference model, is not an average model of an inverter, as the PWM switching pattern is the primary reason for the need of an LCL filter. In this improved model, the input from the controller is converted into a proper PWM signal, as described in chapter 1, section 1.1. This signal is then multiplied by the DC-link voltage to generate a modulated voltage output, almost as a real inverter would make. This model is based the ideal behavior of IGBTs, which does not account for the switching dynamics, like inductive kicks, of IGBTs and is therefore not 100% accurate.

LCL filter model

For the LCL filter the state space model, used in the reference model[15], is reused without any changes. The circuit diagram, as seen on 3.1, shows the general component configuration of an LCL filter.

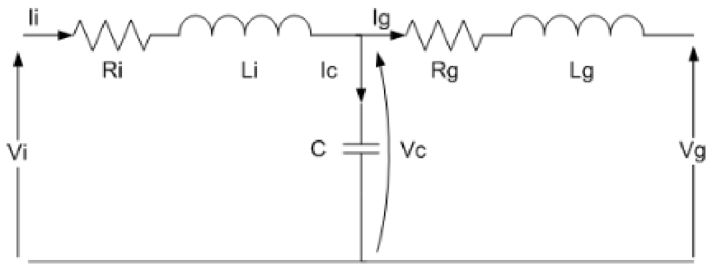

Figure 3.1: Circuit diagram of one of the phases of the LCL filter. [15]

The state space model of the LCL filter has two inputs, three states, and one output. The three states are the input current, the output current, and capacitor voltage. The state space model is described by the equations 3.1 and 3.2. [15]

$$\dot{x} = \begin{bmatrix} \dot{i_{inv}} \\ \dot{i_g} \\ \dot{v_c} \end{bmatrix} = \begin{bmatrix} -\frac{R_i}{L_i} & 0 & -\frac{1}{L_i} \\ 0 & -\frac{R_g}{L_g} & \frac{1}{L_g} \\ \frac{1}{C} & -\frac{1}{C} & 0 \end{bmatrix} \cdot \begin{bmatrix} i_{inv} \\ i_g \\ v_c \end{bmatrix} + \begin{bmatrix} \frac{1}{L_i} & 0 \\ 0 & -\frac{1}{L_g} \\ 0 & 0 \end{bmatrix} \cdot \begin{bmatrix} v_{inv} \\ v_g \end{bmatrix} \tag{3.1}$$

$$y = \begin{bmatrix} 0 & 1 & 0 \end{bmatrix} \cdot \begin{bmatrix} i_{inv} \\ i_g \\ v_c \end{bmatrix} + \begin{bmatrix} 0 & 0 \end{bmatrix} \cdot \begin{bmatrix} v_{inv} \\ v_g \end{bmatrix} \tag{3.2}$$

Grid equivalent load

The grid is modeled by a Thevenin's equivalent grid circuit, as shown on figure 3.2. This model is also a unchanged reuse from the reference model[15].

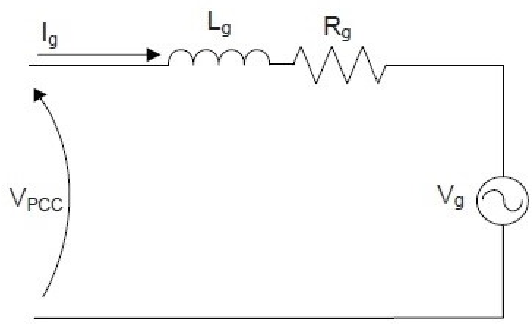

Figure 3.2: Diagram of one of the phases of a Thevenin's equivalent grid circuit. [15]

The RL load in this model is described using equation 3.3. The model require three inputs; the grid voltage, the LCL filter current, and the first derivative of that filter current. The first derivative of the current is extracted from the state vector of the first state space equation in the LCL filter model.

$$v_{load} = R_g \cdot i_g + L_g \cdot \dot{i_g} + v_g \tag{3.3}$$

3.2 Model setup

The model is constructed in Simulink, with the individual component model put into individual, interconnected subsystems as shown on figure 3.3.

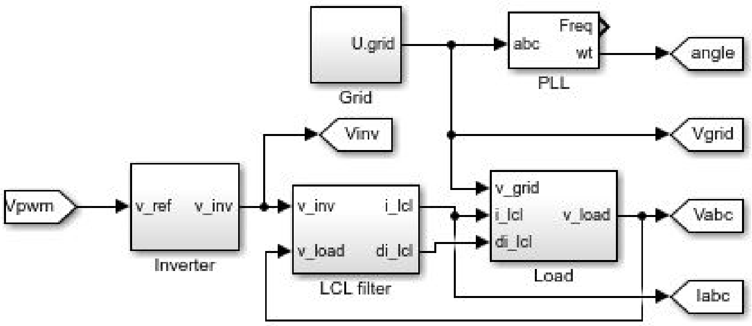

Figure 3.3: Block diagram of the mathematical model.

3.3 Setup specifications

The specifications of the experimental setup, with which the experiments have been conducted, are given in table 3.1. Note that the specifications for the grid equivalent circuit are estimations.

Table 3.1: Model specifications

Constant	Value	Unit
v_{DC}	650	V
f_{sw}	$8 \cdot 10^3$	Hz
R_1	0.1	Ω
L_1	$1.8 \cdot 10^{-3}$	H
R_2	1.4	Ω
L_2	$2 \cdot 10^{-3}$	H
C	$1.404 \cdot 10^{-5}$	F
R_l	2	Ω
L_l	$4 \cdot 10^{-3}$	H
R_g	3.35	Ω
L_g	0.144	H

3.4 Controller design

The controller, used for this model, is a PI current controller. The main feedback measurement is the current output from the filter, which, afterwards, is injected into the grid. As the test setup, modeled in section 3.1, is a Voltage Source Inverter (VSI), the current reference in dq format is calculated from the reference power input and voltage feedback measurement in dq format, using equation 3.4.

$$P = \frac{3}{2} \cdot (v_d \cdot i_d + v_q \cdot i_q) \; , \; Q = \frac{3}{2} \cdot (v_q \cdot i_d - v_d \cdot i_q) \tag{3.4}$$

The output of the PI controller is then added to the voltage feedback measurement to obtain the control output as shown on figure 3.4.

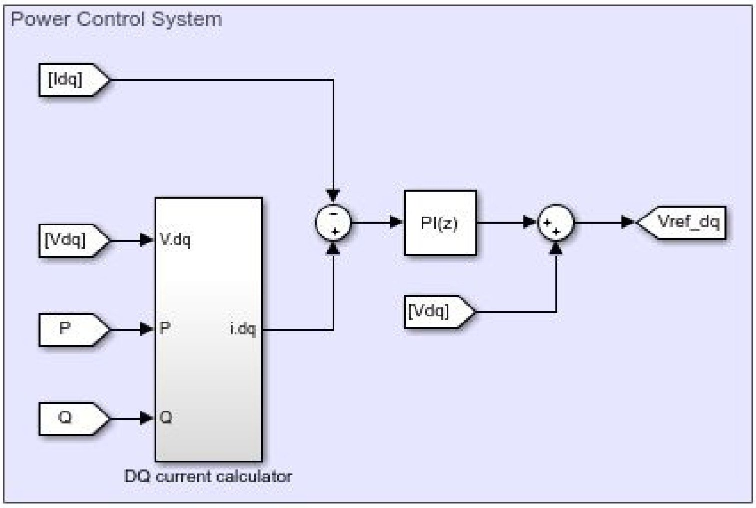

Figure 3.4: The current controller constructed in Simulink.

3.5 Virtual Resistor

This method, as mentioned in chapter 2, section 2.3 the voltage drop across an virtual damping resistor is estimated and then subtracted from the control output. Thereby the behavior of the resistor is imitated without any additional losses, caused by an actual resister being present in the filter. Figure 3.5 shows the circuit of the LCL filter, with the Virtual Resistor placed in series with the capacitor.

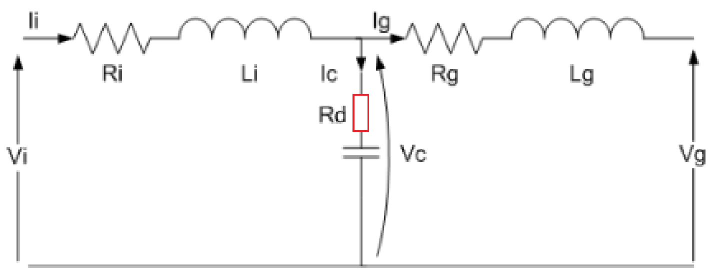

Figure 3.5: Circuit diagram of the LCL filter with visualization of the Virtual Resistor.

Derivation

To estimate the voltage drop across the virtual damping resistor, it is necessary to derive the estimation equations based on the available measurement. The measurements available are the voltages and currents of the grid connected side of the LCL filter. The first step is to estimate the voltage drop across the capacitor, within the LCL filter. This is done using equation 3.5.

$$V_c = V_g + R_g I_g + L_g \frac{\mathrm{d}I_g}{\mathrm{d}t} \tag{3.5}$$

From equation 3.5, the capasitor current can be estimated using equation 3.6.

$$I_c = C \frac{\mathrm{d}V_c}{\mathrm{d}t} \tag{3.6}$$

By combining equation 3.5 and 3.6, equation 3.7 is obtained.

$$I_c = C \frac{\mathrm{d}}{\mathrm{d}t} \left(V_g + R_g I_g + L_g \frac{\mathrm{d}I_g}{\mathrm{d}t} \right) \tag{3.7}$$

Finally equation 3.8 estimates the voltage drop across the virtual resistor.

$$V_R^* = R_d I_c \tag{3.8}$$

Implementation

By implementing the equations 3.7 and 3.8 intro Simulink and subtracting V_R^* from the control output, a system, shown on figure 3.6, is obtained.

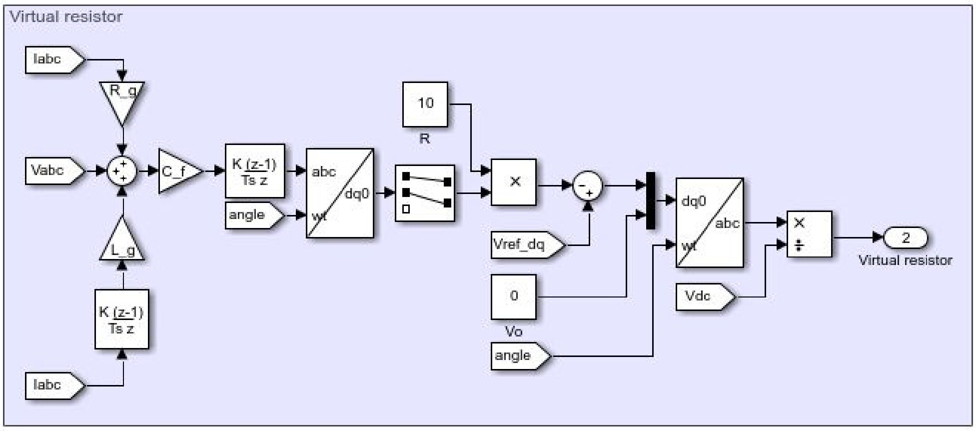

Figure 3.6: The Virtual Resistor constructed in Simulink.

Model test

This test will examine the performance of the model with and without the Virtual Resistor enabled. The test will run for two seconds, and the Virtual Resistor will be enabled at the beginning of the test. After 0.5 seconds, the Virtual Resistor will be disabled, and it will remain disabled for 0.5 seconds, after which it will be re-enabled and remain enabled for the rest of the simulation. The PI controller was tuned, so the gains are $P = 10$ and $I = 100$, and the Virtual Resistance for this simulation is set to 10.

Figure 3.7 shows that the power output gets unstable, when the Virtual Resistor is disabled, and that the power output is stabilized when the Virtual Resistor is re-enabled.
Figure 3.8 shows that the output voltage gets highly distorted, when the Virtual Resistor is disabled. This can also be seen on figure 3.9. Here the THD curve is very unstable, and spikes in both the voltage and current THD exceed 160%. When the Virtual Resistance is re-enabled, control is immediate regained, and the THDs and voltage output returns to an acceptable level after 0.2 seconds.

The conclusion of this test is that the Virtual Resistor works for the simulation model. Under real conditions the system will probably have a slower reaction time, and that the behavior of the system is therefore more modest with less distortion and smaller spikes.

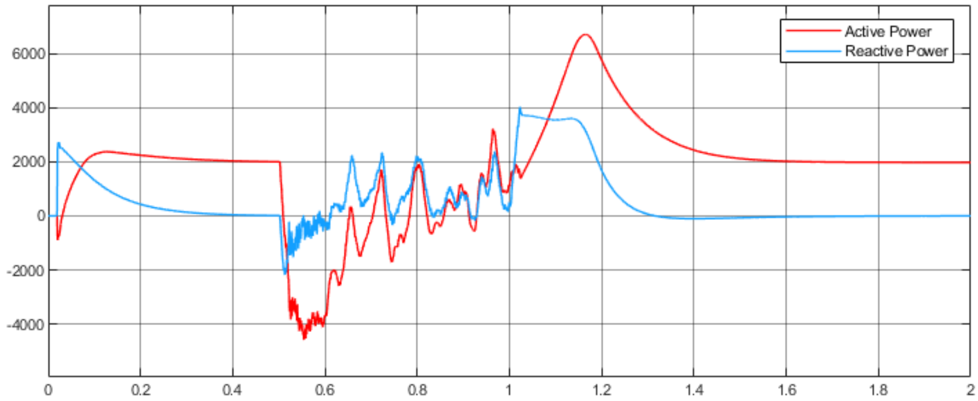

Figure 3.7: The power output from the inverter during the test

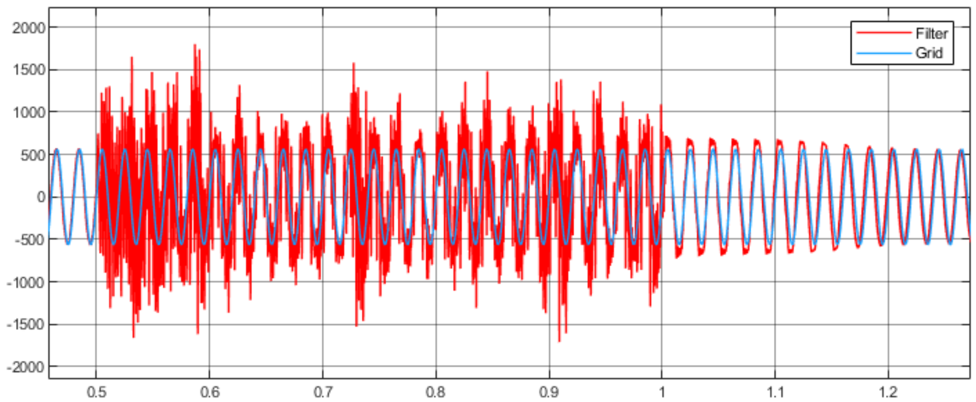

Figure 3.8: The voltage output during the test compared to the grid voltage

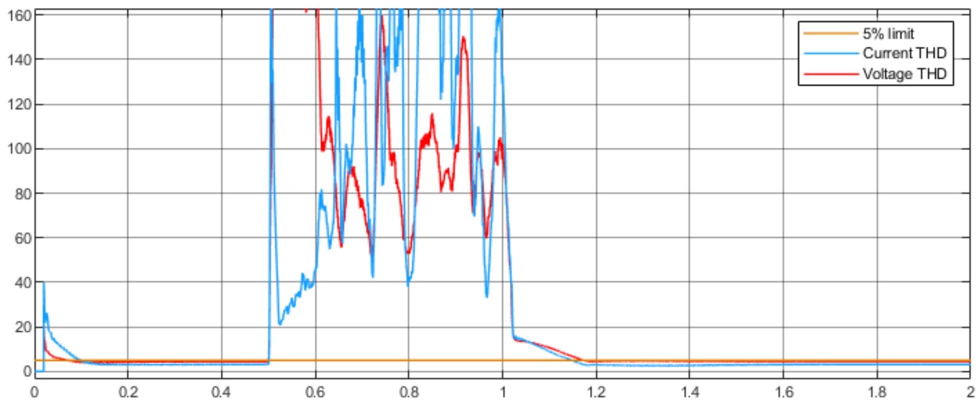

Figure 3.9: The voltage and current THDs during the test in percent

Chapter 4

Adaptive Virtual Resistance

The optimal Virtual Resistance under consistent nominal operation will remain constant, but for renewable energy-producing, grid-connected, devices the operation conditions are dynamic due to various factors. The power output and grid conditions change constantly, which affects the currents running inside the inverter and filter, and thereby the harmonic currents. Therefore it can be assumed that the optimal Virtual Resistance will not be the same under all operational conditions.

4.1 Test of various operational conditions

To test this with the model, described in section 3.1, a series of tests are performed at various operational conditions, where the reference power and Virtual Resistance is changed. The test simulations are run until a steady state is obtained.

Table 4.1: Model specifications

Virtual	Current THD			Voltage THD		
Resistance	500 W	1000 W	2000 W	500 W	1000 W	2000 W
8	9.7 %	5.1 %	4.2 %	4.4 %	4.4 %	4.8 %
10	8.5 %	4.5 %	3.2 %	4.3 %	4.3 %	4.5 %
12	7.9 %	4.1 %	2.7 %	4.2 %	4.2 %	4.3 %
14	7.5 %	3.9 %	2.3 %	4.2 %	4.2 %	4.2 %
16	7.3 %	3.7 %	2.1 %	4.1 %	4.1 %	4.2 %
18	7.1 %	3.6 %	1.9 %	4.1 %	4.1 %	4.2 %
20	7.0 %	3.6 %	1.8 %	4.1 %	4.1 %	4.2 %
22	6.9 %	3.5 %	1.8 %	4.1 %	4.1 %	4.2 %
24	6.9 %	3.5 %	1.7 %	4.1 %	4.1 %	4.1 %
26	7.0 %	3.5 %	1.7 %	4.1 %	4.1 %	4.1 %
27	7.2 %	3.7 %	1.8 %	4.2 %	4.1 %	4.2 %
28	27.5 %	14.2 %	7.5 %	14 %	13.7 %	13.1 %

Table 4.1 shows that voltage THD is at a stable level in the majority of the tests, while the current THD is varying more. Based on the results, it can be concluded for this model, that the optimal Virtual Resistance is in the range between 22 and 26. The results for the 500 W power reference shows, that the optimal Virtual Resistance

would be approximately 23, while it would be approximately 24 at 1000 W and 25 at 2000 W. In a real test, where the distortion would be greater, it would be assumed that the differences would be more significant.

Furthermore, the test shows that there is a point of instability, if the Virtual Resistance is increased too much. In these tests the point of instability is at a Virtual Resistance of 28. When increasing the Virtual Resistance, the controllability of the system will decrease, as seen on figure 4.1 and figure 4.2. These two figures show that an increase in the Virtual Resistance will result in a larger overshoot and a longer settling time of the system.

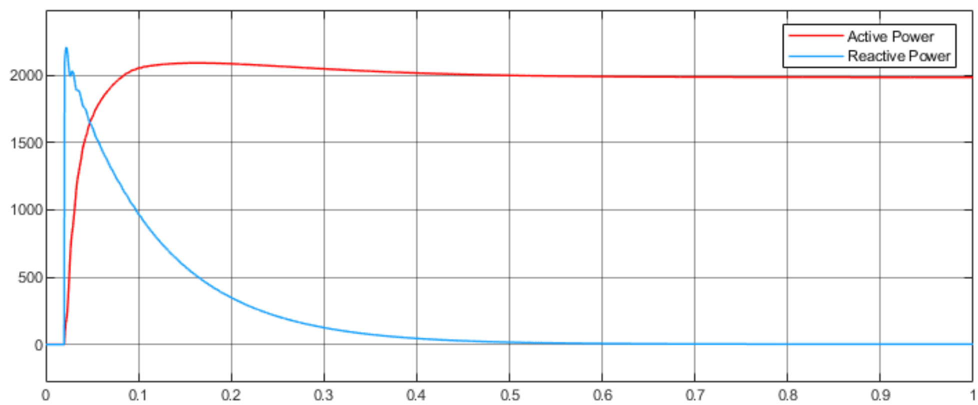

Figure 4.1: The power output with a Virtual Resistance of 8.

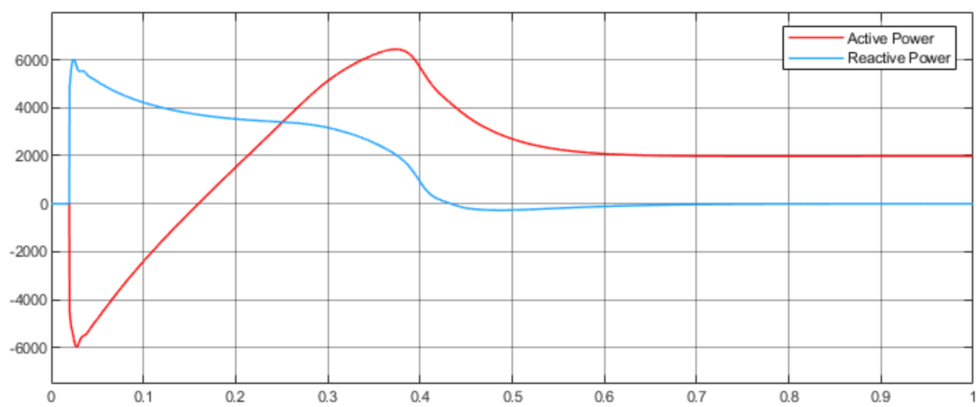

Figure 4.2: The power output with a Virtual Resistance of 24.

The behavior of the modeled system does presumably not reflect real behavior to the extent, shown on figure 4.1 and 4.2, but it can be concluded that a lower Virtual Resistance will decrease overshoots and settling time, and is therefore desirable under conditions, where there is a large difference between the reference and feedback values in the system.

4.2 Minimal Distortion Tracking for optimal resistance

As shown in section 4.1, the optimal Virtual Resistance increase when the power output increase. In this test the power output quadrupled, but for most renewable energy-producing devices the power output range is larger. Therefore the range of optimal Virtual Resistance will be significant, and from that it can be assumed, that tracking the optimum could improve the overall performance of the inverter.

A well known tracking algorithm, Maximum Power Point Tracking (MPPT), is known for tracking the optimal power output from a photovoltaic solar panel. This algorithm is tracking the optimum based on two variables; the power output and voltage of the solar panel. The voltage is controlled by the algorithm and the change in power output is tracked in order to maximize the power output. Figure 4.3 shows the characteristics of a solar panel.

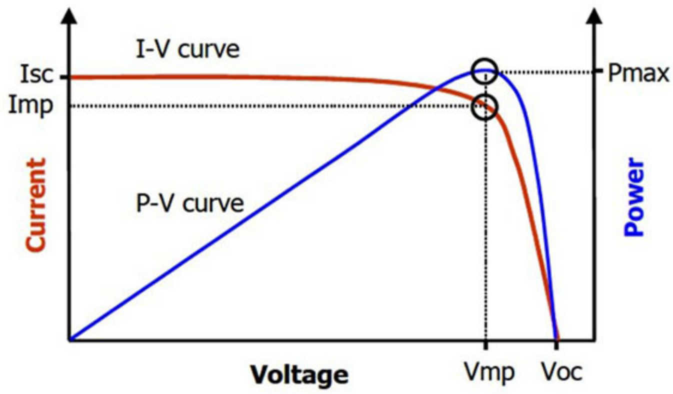

Figure 4.3: The voltage-current (red) and voltage-power (blue) relationship for a PV solar panel.[14]

To adapt the MPPT algorithm for the purpose of tracking the least amount of distortion, the THD is the tracked variable, and the Virtual Resistance is the control variable. The flowchart on figure 4.4 shows the overall concept of the tracking-algorithm.

Two important design parameters of the tracking algorithm is the sample time of the algorithm, and the step size per sample. These two parameters must be designed to fit with the specific setup, as systems have a settling time, in which the system must settle before a new change is made. The step should also result in a measurable change, so the step size and sample time must be tuned with regards to each other, to obtain the optimal tracking results.

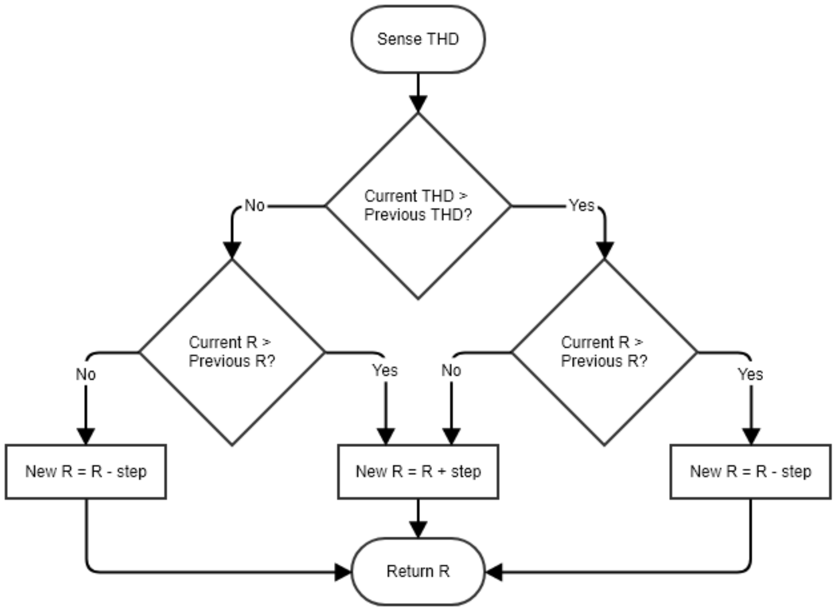

Figure 4.4: Flow diagram of the algorithm for tracking minimal distortion.

As mentioned in section 4.1, a large Virtual Resistance is not desirable during the start-up sequence, so as an initial condition of the Virtual Resistance should be a value, which is optimal for the start-up sequence, but still manage to keep the harmonic distortion to an acceptable level. When the start-up sequence is completed the Minimal Distortion Tracking can be enabled. If the Virtual Resistance should disturb the controller of the inverter, additional measures could be implemented to further improve the algorithm.

4.3 Testing the Minimal Distortion Tracking algorithm

In this section the algorithm will be implemented into Simulink, tested and, based on the test results, the algorithm will be further improved.

Implementation into Simulink

The implementation into Simulink is primarily done by using a MATLAB function block, which contain the algorithm, shown in the flowchart on figure 4.4. The full implementation of the algorithm into Simulink is shown on figure 4.5.

To obtain the current THD, which is the THD is used in this tracker, a THD block from the Simulink library was used, and the input for that block is a three-channel

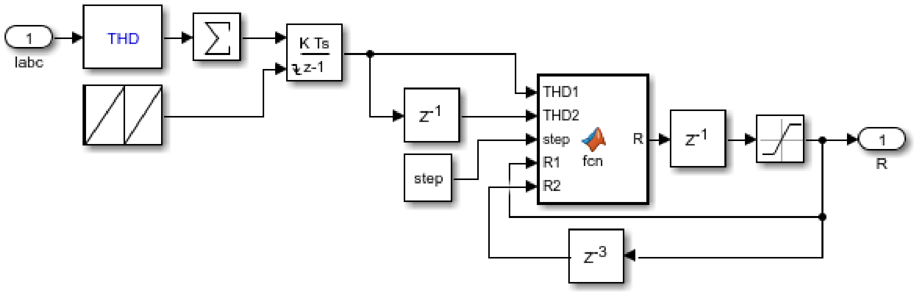

Figure 4.5: The Minimal Distortion Tracking algorithm implemented into Simulink.

signal of the measured three-phase current. The output is a three-channel signal of the THD, which is combined into a single channel by the sum block. The original intention after this was to divide the signal by 3 to obtain the average THD, but since that would not benefit the algorithm, but only add an extra computation, this action was left out.

The next operation is an integrator block, which accumulate the THD data from the entire sample to obtain a THD value, which is representing the whole sample, and not just the final value of the sample. This is especially useful for systems with fluctuating current THD, as the final value could otherwise be either the top or valley of a fluctuation, and therefore misrepresent the THD of the sample. After each sample, the integrator value is reset zero, and new data can be accumulated.

The rest of implementation is the MATLAB function block and delay blocks, which delay the signals one sample in order to use them at the values from the previous sample. The delay block and saturation block, at the output the MATLAB function block, is to implement the initial condition, as the function block itself has no such option.

First test

The first test is conducted with a simulation time of 5 seconds, a sample time 1 second and a step size of 1. The initial Virtual Resistance is set to 8, and the reference power output is 2000 W. This is to examine the behavior of the system with the algorithm implemented.

This test shows that the instantaneous change of Virtual Resistance, shown on figure 4.6, results in disruption spikes in both power output and THD, as shown on figure 4.7 and 4.8, each time the Virtual Resistance is changed. This behavior is not desirable, as it create unnecessary disruption of the output.

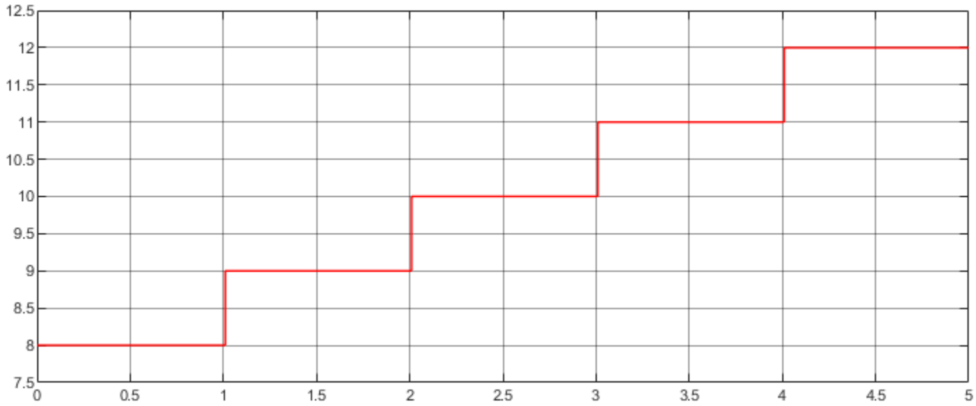

Figure 4.6: The change in Virtual Resistance during the first test.

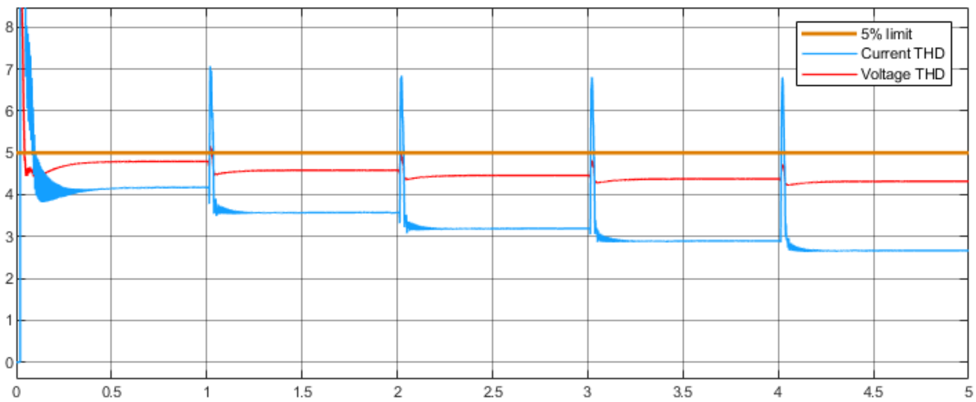

Figure 4.7: The THD during the first test.

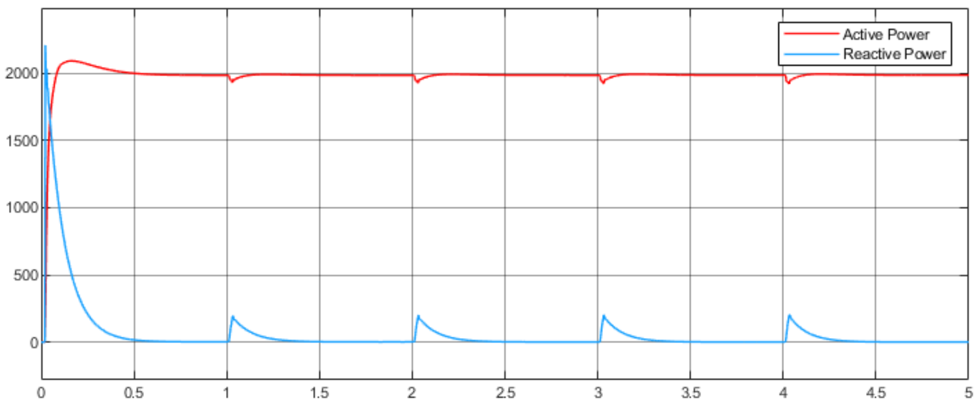

Figure 4.8: The power output during the first test.

Improved algorithm and second test

To avoid disruptive spikes, caused by the instantaneous change of Virtual Resistance, a feature is introduced to create a gradual change in the Virtual Resistance at the output of the Simulink implementation. A 'Rate Limiter' block is added to limit the rate of change of the output. The maximum rate of change design in such a way, that the change can be completed in the first half of a sample. Furthermore, as the first half of the sample is now reserved for the Virtual Resistance to change, only the current THD, from the second half of the sample, will be useful for comparison. The integrator block will therefore be resat in the middle of each sample, as well as at the end.

A test of the improved tracking algorithm is now performed under the same conditions as the previous test.

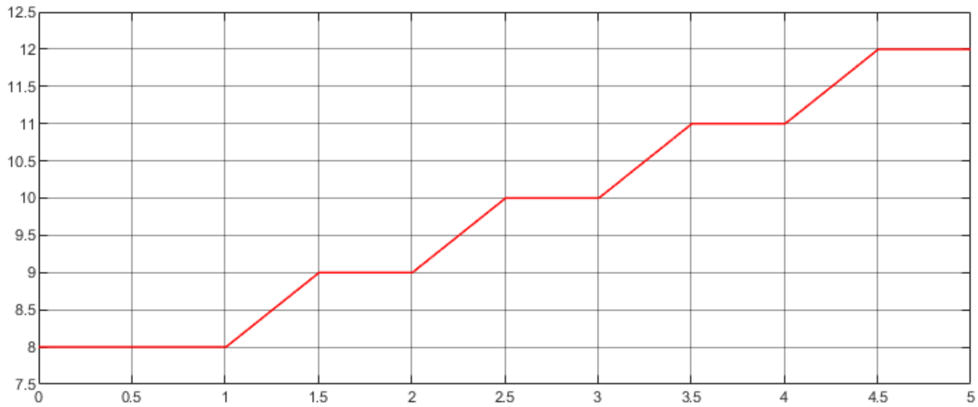

Figure 4.9: The change in Virtual Resistance during the second test.

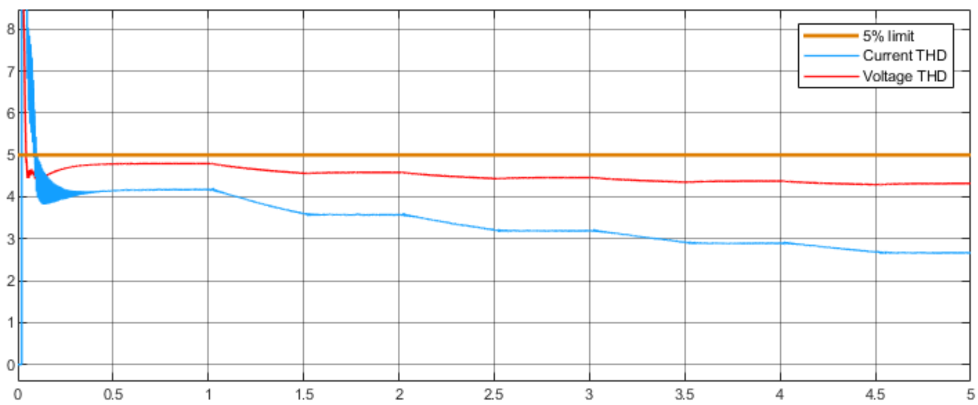

Figure 4.10: The THD during the second test.

This test, with the before described improvements, shows that the gradual change

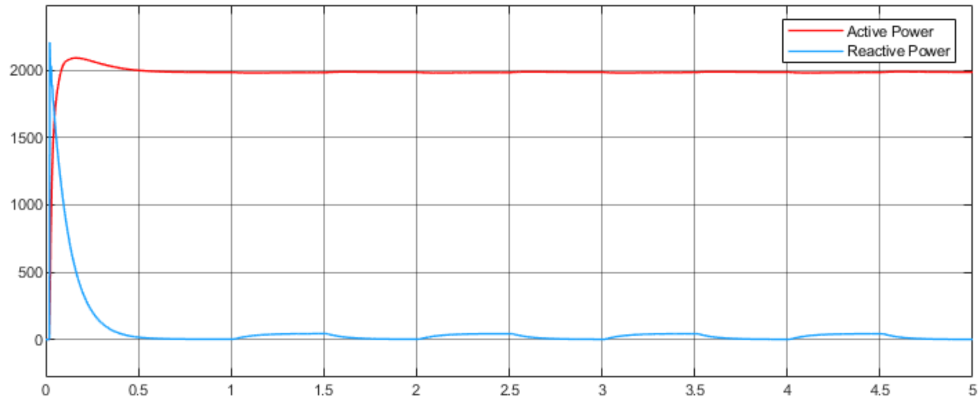

Figure 4.11: The power output during the second test.

of Virtual Resistance, shown on figure 4.9, results in a more stable power output with only the reactive power output being significantly affected. This can however be minimized through fine tuning of the system.

Third test

To verify that the Minimum Distortion Tracking algorithm is functioning effectively this test is run for 30 seconds, under the same conditions as during the second test. The power output is set to 2000 W, the sample time is 1 second and the initial Virtual Resistance is set to 8. For this test to be successful, the algorithm should find an optimal Virtual Resistance around 25, as the results of the test in section 4.1 indicates.

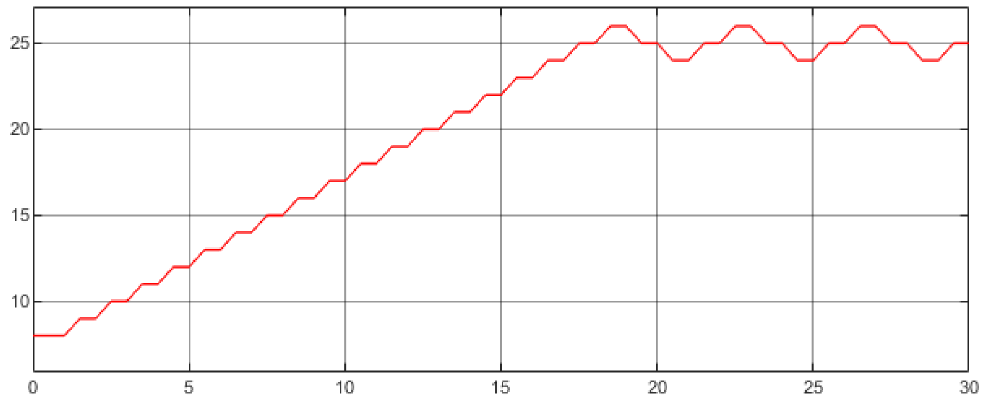

Figure 4.12: The change in Virtual Resistance during the third test.

As shown on figure 4.12, the Virtual Resistance during this test settles around

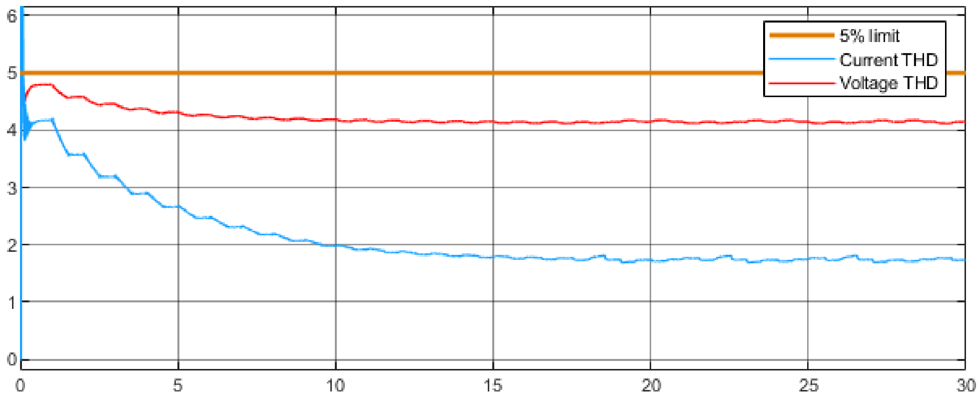

Figure 4.13: The THD during the third test.

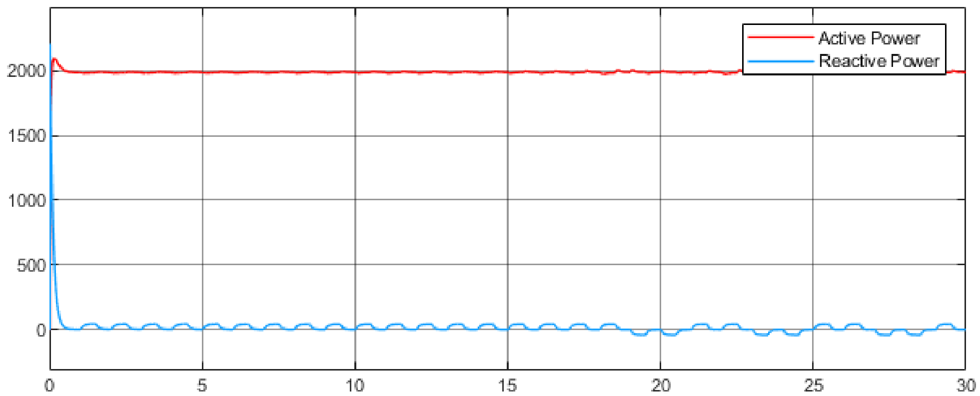

Figure 4.14: The power output during the third test.

25. Figure 4.13 shows the initial decrease in distortion, and that the algorithm is able to maintain the lowest possible level of distortion. Figure 4.14 shows a stable output of active power, while the reactive power has small fluctuations. This can, as mentioned before, be minimized through fine tuning of either the controller or algorithm settings.

4.4 Conclusion

From the tests and improvements, described in section 4.3 it can be concluded that the Minimal Distortion Tracking algorithm is able to effectively track the optimal Virtual Resistance. The algorithm could be further improved by e.g. adding a variable step size feature to improve the tracking speed of the algorithm.

Chapter 5

Lab Testing

5.1 Inverter setup

The inverter setup, used for the tests of the control system, is an already existing setup built by the Department of Energy Technology in Aalborg. It contains Danfoss drive, a dSpace control module, an LCL filter, with the specifications described in chapter 3, section 3.3, and other components like breakers and sensors etc. The DC voltage is supplied by a separate voltage supply from Delta Elektronika. The complete setup is shown on figure 5.1.

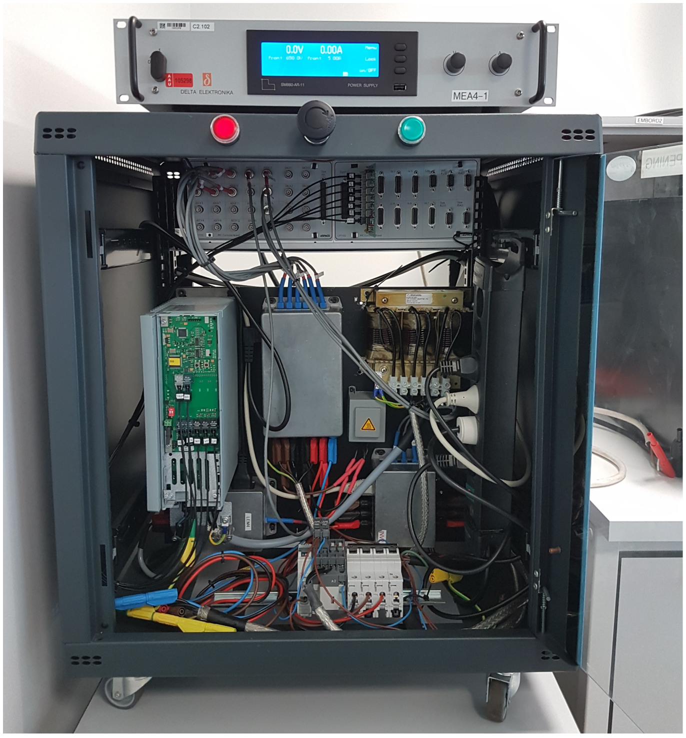

Figure 5.1: The inverter used for the experiments.

To avoid a complete short circuit of the setup, the dSpace controller is connected to the Danfoss drive through fiber optic cables. These ensure that the two components are completely electrically separated, so a short circuit in one component, does not result in the malfunction of both.

5.2 Implementation

The designed PI control system with Virtual Resistance has been implemented into an already existing control system, designed for the specific inverter setup. The control system, which was provided with the inverter setup, contains a PI controller with harmonic compensation for the 5th and 7th harmonic components. The system also uses 3rd harmonic injection to further improve the performance of the control system.

The main disadvantage with the Virtual Resistor method is that it requires a double derivative, which, under normal circumstances, is sensitive to noisy measurements. To minimize this problem, a discrete time filtered derivative is used.

Discrete-time filtered derivative

To address the noise problem with normal discrete time derivatives, a page was found on mathworks.com [12], which poorly described a filtered derivative method. Furthermore, the web page also contained a picture of a Simulink setup, a graph showing the performance of the filtered derivative, and a link to the file, which was depicted on the page. Based on the graph, it was decided that the method should be further investigated.

The transfer function, within the provided file, was a derivative with a built-in filter in a transfer function. The transfer function is shown as equation 5.1, where ζ is a damping factor between 0 and 1, and T_s is the sample time of the discrete-time derivative.

$$G(z) = \frac{(1-\zeta)\cdot(z-1)}{T_s\cdot(z-\zeta)} \tag{5.1}$$

This method was tested in Simulink, and figure 5.2 shows the result of a test with a filter damping factor of 0.85. The test shows that the filtered derivative has less fluctuations than the unfiltered, but a phase shift occur, and another test with a higher damping factor shows that the peak amplitude of the filtered derivative is also lowered, in comparison to the reference derivative.

The conclusion with this method is that the lower amplitude can be counteracted by an increase in the Virtual Resistance, and that tests will show if the phase shift will become an issue.

Controller implementation

As the provided control system already contains the framework for the implementation of the controller, designed in chapter 3, section 3.4, the only major change to the system was to replace the harmonic compensator with the Virtual Resister. Most

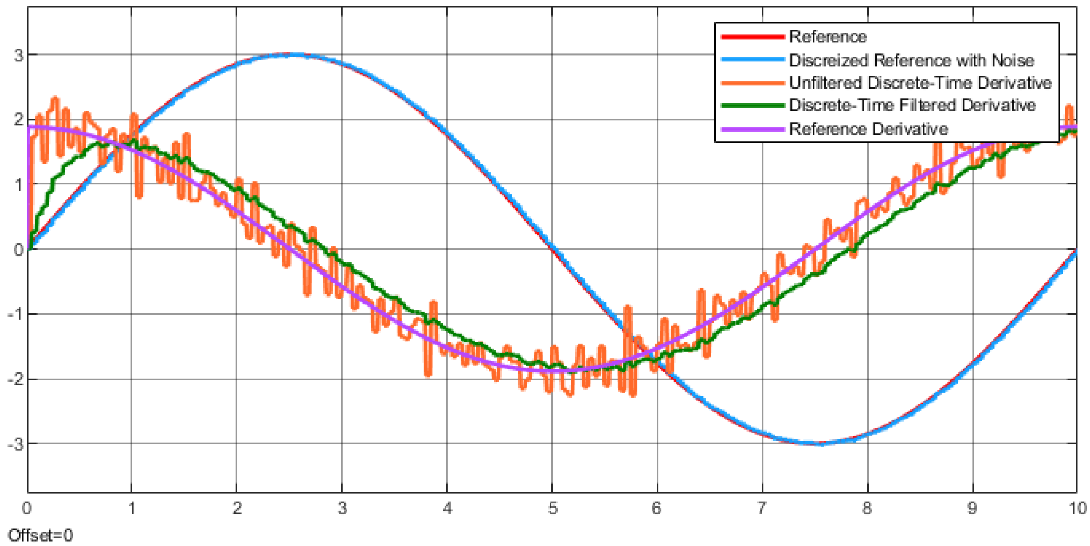

Figure 5.2: A scope from a test of the discrete-time filtered derivative with comparisons.

of the control system consist of dSpace communication and signal processing, which is essential for the controller to work. Therefore these parts of the controller has not been modified. Figure 5.3 shows the controller setup in Simulink, where the current controller has been modified, and the necessary signal transformation operations have been implemented.

dSpace Control Desk interface

With the provided control system, there is also an interface for the dSpace Control Desk software, shown on figure 5.4. This interface also went through some minor modifications, where the harmonic compensator control interface was modified into an interface for the Virtual Resister.

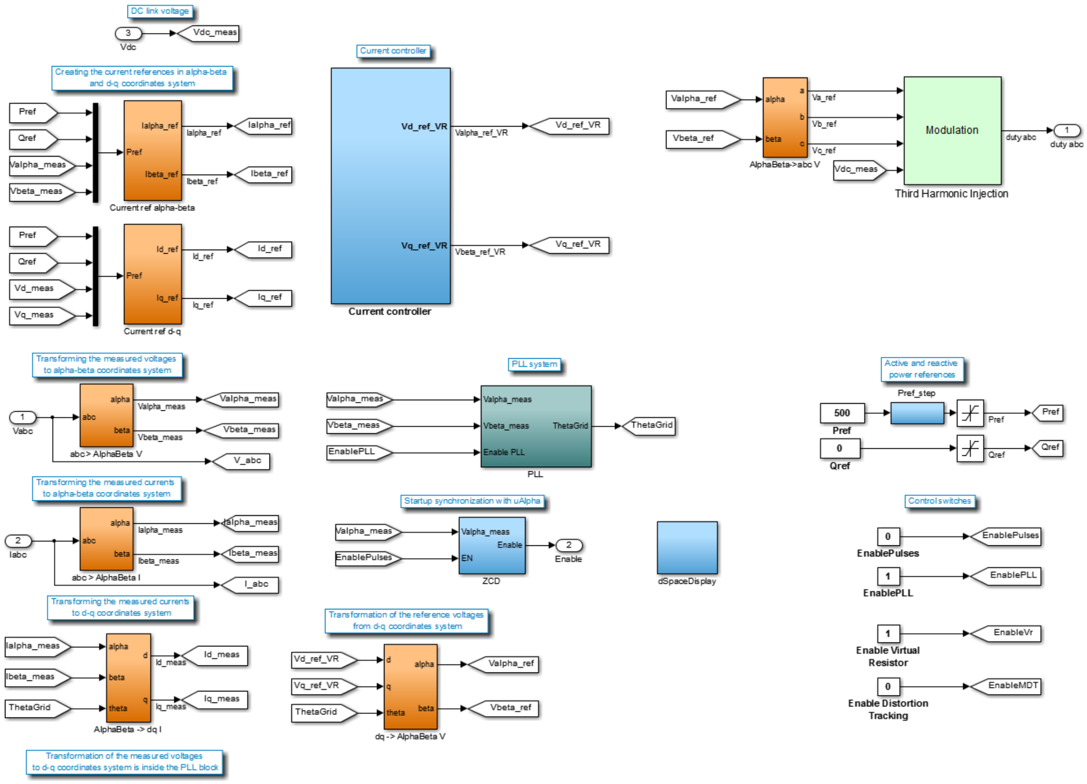

Figure 5.3: The controller setup for the inverter, constructed in Simulink

5.3 Optimization

When the implementation process was almost completed, before the discrete-time filtered derivative was added, the use of a normal discrete-time derivative resulted in the Virtual Resistor having no damping effect on the system. Afterwards, when the discrete-time filtered derivative was implemented, the first test was conducted with a damping factor of 0.6, the Virtual Resistor managed to reduce the current THD with one 10th of the unfiltered distortion at different power outputs. This initial test showed that designed the Virtual Resister worked, but that optimization was needed. Due to limitations in the Simulink software, the only possible sample time, T_s, of the discrete-time filtered derivative was the one corresponding to the 8 kHz switching frequency; 0.125 ms. Therefore, it has not been possible to conduct tests at any other sample time.

The optimization process was conducted by running a series of tests with different damping factors. At each test the Virtual Resistance was adjusted manually to obtain the lowest current THD possible. In table 5.1 the results of these tests are shown.

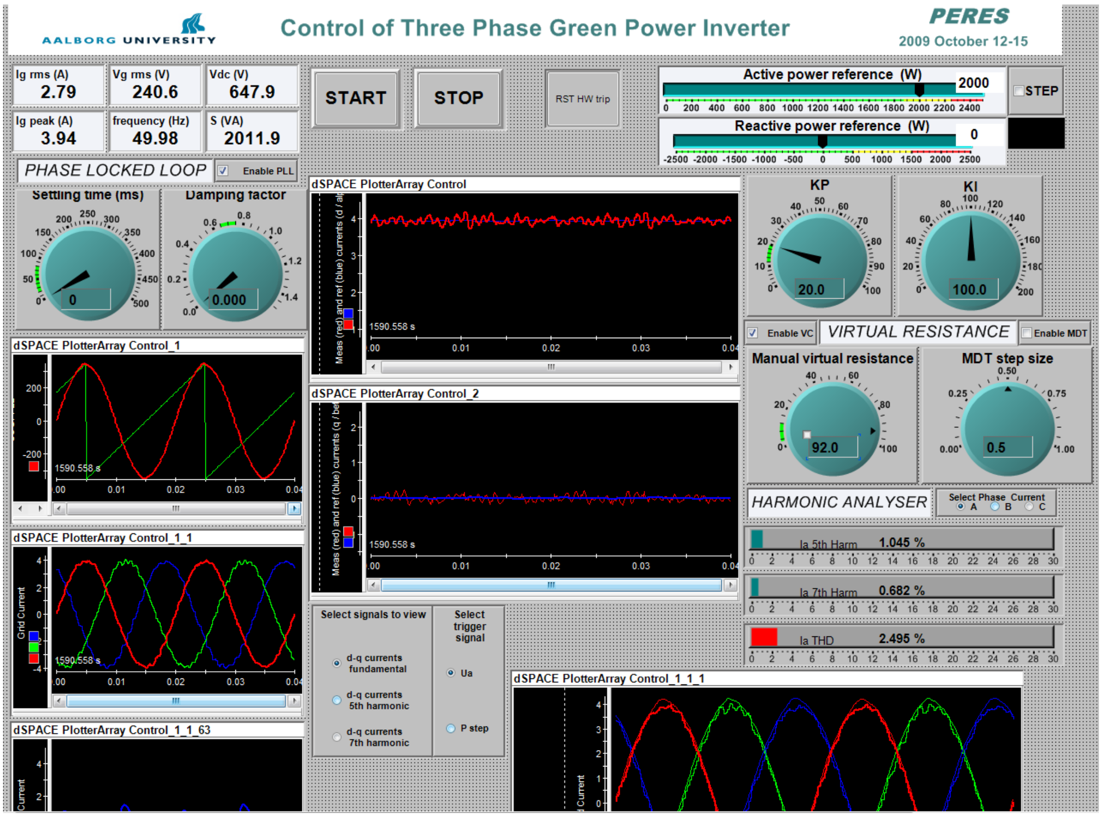

Figure 5.4: The modified inverter interface in dSpace ControlDesk.

Table 5.1: The results of the optimization tests

Test	DF	Current THD at			Virtual Resistance at		
		500 W	1000 W	2000 W	500 W	1000 W	2000 W
1	0.6	16.0 %	11.0 %	6.3 %	7	7	7
2	0.65	16.4 %	10.5 %	6.1 %	10	10	10
3	0.7	16.1 %	9.8 %	5.7 %	15	17	20
4	0.75	14.5 %	8.2 %	4.7 %	20	23	28
5	0.8	13.7 %	7.8 %	4.1 %	27	35	39
6	0.85	13.0 %	7.0 %	3.7 %	36	48	58
7	0.9	12.4 %	6.1 %	3.1 %	58	74	86
8	0.95	12.1 %	5.9 %	3.1 %	110	155	165
9	0.99	13.1 %	6.8 %	3.5 %	650	840	800

Based on the results of the optimization, it can be concluded that the optimal damping factor of this Virtual Resistor is within the range of 0.90 to 0.95. Furthermore, in response to the concerns described under Discrete-time filtered derivative in section 5.2, it can be concluded that the phase shift in these filtered derivatives did not have a significant effect on the efficiency of the Virtual Resistor. This might be due to the small sample time, but it was not, as mentioned before, possible to test otherwise with the current setup. It can also be concluded, that the decrease in amplitude of the filtered derivatives was counteracted by an increase in the Virtual Resistance without amplifying remaining noise to a degree, that would cause destabilization.

Finally, the results confirm the assumption from chapter 4, section 4.1, that the difference in optimal Virtual Resistance, at different operational conditions, would be more significant under real conditions. Therefore, implementation of a Minimal Distortion Tracking algorithm could greatly enhance the performance of this inverter control system.

5.4 Validation test

In this section, the final validation experiment will be described, and results from the lab setup and simulation model will be compared. The experiment will consist of a series of tests with varying reference power input. The optimal Virtual Resistance is obtained, in the lab through manual adjustment, and in the simulation by Minimal Distortion Tracking. For this experiment, the integration damping factor is set to 0.90, within the Virtual Resistance estimation in the lab setup.

Table 5.2: The results of the validation tests

Test	Reference power		Lab. result		Sim. result	
	Active	Reactive	VR	THD	VR	THD
1	500	0	48	12.9 %	23	6.9 %
2	500	500	72	10.8 %	17	6.0 %
3	500	-500	76	8.5 %	27	4.0 %
4	1000	0	74	6.2 %	24	3.5 %
5	1000	500	68	6.5 %	17	3.9 %
6	1000	1000	66	5.3 %	13	4.1 %
7	1000	-500	64	5.5 %	27	2.6 %
8	2000	0	92	2.5 %	25	1.7 %
9	2000	500	70	4.2 %	18	2.2 %
10	2000	1000	62	3.5 %	14	2.9 %
11	2000	-500	74	3.2 %	27	1.4 %
12	2000	-1000	56	3.4 %	27	1.0 %

On table 5.2 the results show, that there is no apparent correlation between the optimal Virtual Resistance in the tests, but a clear correlation between the THD results. On figure 5.5, where the THD results from the simulations have been scaled up by a factor of 2, a correlation can clearly be seen. The correlation coefficient for these results is 0.94, which further confirms this correlation.

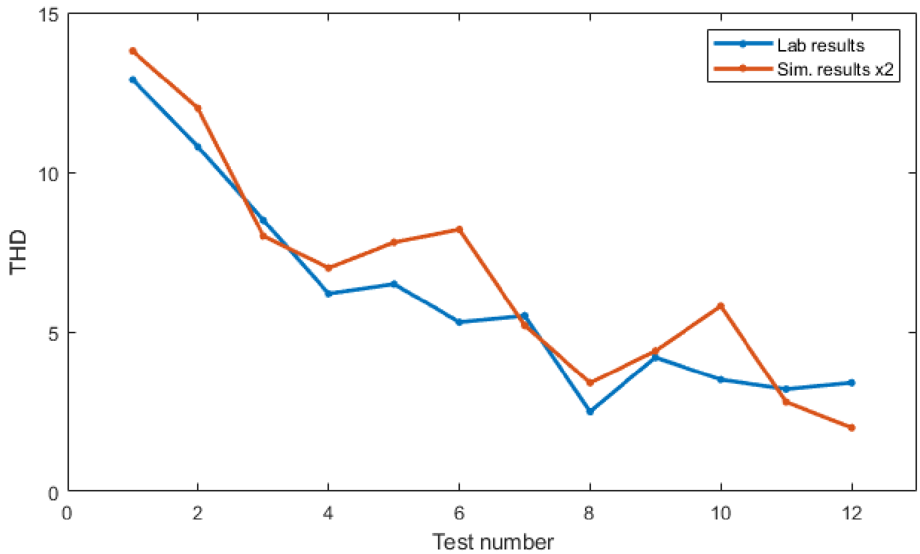

Figure 5.5: The THD results of the validation experiment, with the simulations results scaled up by two.

From these results, even though the optimal Virtual Resistance results were not clearly correlated, the model behavior matches the behavior of the lab setup to a degree, where it can be concluded that the model is valid.

Discussion

First of all the choice of the Virtual Resistor over the PR controller and Notch filter was based on the fact, that the Virtual Resistor seemed more robust to external grid influences. As this claim has not been tested, the truth of the claim will remain unknown. Furthermore, no literature was found with a definitive answer to, which method is the best for grid-connected applications, as all the papers had slightly different approaches, several only compared with standard approaches to competing methods, and some did not document the testing procedures as well as others. Most results were presented at graphs and scopes, and very few numbers were presented, which further complicates the comparison. For future reference, these methods should be tested head to head under similar conditions, with well documented testing procedures and with comparable results like THD or similar values.

Among the papers, presented in the review, few presented THD measurements, and of those only one was comparable to the best results, achieved during the testing phase, which would indicate that the experimental results, and thereby also the implemented control system works to a satisfactory degree. The requirement of less than 5% THD was met in all the test at 2000 W, and the correlation between the predicted and actual behavior of the system was satisfactory as well. The predicted THDs was approximately half of the actual ones, which could be caused by some of the distortion, caused by the switching dynamics of the inverter, not being accounted for in the model. Another reason could be the estimated grid impedance, which can be difficult to estimate. These factors could account for most of the margin of error, but the overall model seems valid anyway.

The implementation of the PI controller and Virtual Resistor went well due to the filtered discrete-time filtered derivative, which ensured that the double derivative of the Virtual Resistance worked despite noise in the measurements. This problem was mentioned in many papers, but none of the papers seemed to use any method similar to this one. The test results showed that the method was effective, but if the results are compared to results from the 8th semester project in the appendix, where a two-loop controller with harmonic compensation was used, the results for all reference power outputs, except the 2000 W test, had a smaller THD than the results in these tests. This could indicate that the Virtual Resistance method works best under higher power outputs.

Even though the concept of Adaptable Virtual Resistance was documented in one paper, the approach with a Minimal Distortion Tracking algorithm seems very different from the method, described in that paper. The Minimal Distortion Tracking seems like a promising addition to the concept of Adaptable Virtual Resistance. Due to time constraints and setup problems, the MDT algorithm was not implemented into the lab. control system. The problem with the sample time, described in chapter 5, section 5.3, also affected the implementation of the algorithm, as error messages of asynchronous behavior kept occurring throughout the implementation attempts. This is, however, only a problem with the Matlab/Simulink environment, and not a problem with the algorithm itself, and it will therefore be possible to implement into other environments, and maybe also Matlab/Simulink, if the right solution to the problem is found.

However, even though the algorithm has not been implemented into the controller of the lab setup, the mindset behind the algorithm suggests that it would work as intended, as the base algorithm has several similarities with the manual adjustment, used for the experiments.

The wider reaching effect of this, or any other, active damping method is, that the need for passive damping resistors is replaced by smarter control systems, and thereby the power losses and affiliated need for cooling of damping resistors is no longer present. This will result in a more efficient and cost effective Voltage Source Inverters, which is highly desirable on a growing market for power electronic converters.

Conclusion

The overall conclusion of this project is that a PI control system with Virtual Resistance has been designed, tested and predominantly works as intended. The implementation of the designed control system and especially the Virtual Resistance proved successful, by using discrete-time filtered derivatives to tackle the problem of double derivatives and noisy measurements.

The Minimal Distortion Tracking algorithm has shown a potential to become a great addition to the concept of Adaptable Virtual Resistance, even though it has yet to be properly tested on a real inverter control system.

Bibliography

[1] S. V. Araujo et al. "LCL filter design for grid-connected NPC inverters in offshore wind turbines". In: *Proc. 7th Internatonal Conf. Power Electronics*. Oct. 2007, pp. 1133–1138. DOI: 10.1109/ICPE.2007.4692556.

[2] F. Blaabjerg et al. "Overview of Control and Grid Synchronization for Distributed Power Generation Systems". In: *IEEE Transactions on Industrial Electronics* 53.5 (Oct. 2006), pp. 1398–1409. ISSN: 0278-0046. DOI: 10.1109/TIE.2006.881997.

[3] S. Bosch, D. Lebsanft, and H. Steinhart. "Self-adaptive resonance frequency tracking for digital notch-filter-based active damping in LCL-filter-based active power filters". In: *Proc. 19th European Conf. Power Electronics and Applications (EPE'17 ECCE Europe)*. Sept. 2017, P.1–P.10. DOI: 10.23919/EPE17ECCEEurope.2017.8099104.

[4] M. Büyük et al. "A notch filter based active damping of llcl filter in shunt active power filter". In: *Proc. Int. Symp. Power Electronics (Ee)*. Oct. 2017, pp. 1–6. DOI: 10.1109/PEE.2017.8171701.

[5] H. H. Figueira et al. "Brazilian grid-connected photovoltaic inverters standards: A comparison with IEC and IEEE". In: *Proc. IEEE 24th Int. Symp. Industrial Electronics (ISIE)*. June 2015, pp. 1104–1109. DOI: 10.1109/ISIE.2015.7281626.

[6] H. Ge et al. "Research on LCL filter active damping strategy in active power filter system". In: *Proc. Identification and Control (ICMIC) 2017 9th Int. Conf. Modelling*. July 2017, pp. 476–481. DOI: 10.1109/ICMIC.2017.8321691.

[7] W. Ghzaiel et al. "A novel grid impedance estimation technique based on adaptive virtual resistance control loop applied to distributed generation inverters". In: *Proc. 15th European Conf. Power Electronics and Applications (EPE)*. Sept. 2013, pp. 1–10. DOI: 10.1109/EPE.2013.6631966.

[8] *IEEE Standard for Interconnection and Interoperability of Distributed Energy Resources with Associated Electric Power Systems Interfaces*. IEEE Standards Association, Apr. 2018. DOI: 10.1109/IEEESTD.2018.8332112.

[9] K. Koiwa et al. "Sensorless virtual resistance damping method for grid-connected three-phase PWM converter with LCL filter". In: *Proc. Int. Conf. Electrical Machines and Systems (ICEMS)*. Oct. 2013, pp. 1746–1749. DOI: 10.1109/ICEMS.2013.6713280.

[10] Y. Lei et al. "An improved virtual resistance damping method for grid-connected inverters with LCL filters". In: *Proc. IEEE Energy Conversion Congress and Exposition*. Sept. 2011, pp. 3816–3822. DOI: 10.1109/ECCE.2011.6064287.

[11] M. Liserre, F. Blaabjerg, and S. Hansen. "Design and control of an LCL-filter-based three-phase active rectifier". In: *IEEE Transactions on Industry Applications*

41.5 (Sept. 2005), pp. 1281–1291. ISSN: 0093-9994. DOI: 10.1109/TIA.2005.853373.

[12] MathWorks. *Discrete-Time Derivative of Floating-Point Input*. Last accessed: May 2019. URL: www.mathworks.com/help/simulink/slref/discrete-time-derivative-of-floating-point-input.html.

[13] *Photovoltaic (PV) systems - Characteristics of the utility interface*. International Electrotechnical Commission, Dec. 2004. URL: webstore.iec.ch/publication/5736.

[14] Power Electronics Sam Davis. *Solar System Efficiency: Maximum Power Point Tracking is Key*. Last accessed: May 2019. Dec. 2015. URL: www.powerelectronics.com/solar/solar-system-efficiency-maximum-power-point-tracking-key.

[15] Hisham Hasan Taleb, Waqas Aslam Cheema, and Mikkel Rindholt. *Power Control of Grid Connected Converter for Offshore Wind Power System*. 8th semester project report - Found in appendix. June 2018.

[16] C. Tarasantisuk et al. "Active and reactive power control for three-phase grid inverters with proportional resonant control strategies". In: *Proc. Telecommunications and Information Technology (ECTI-CON) 2016 13th Int. Conf. Electrical Engineering/Electronics, Computer*. June 2016, pp. 1–6. DOI: 10.1109/ECTICon.2016.7561379.

[17] R. Teodorescu et al. "Proportional-resonant controllers and filters for grid-connected voltage-source converters". In: *IEE Proceedings-Electric Power Applications* 153.5 (Sept. 2006), pp. 750–762. ISSN: 1350-2352. DOI: 10.1049/ip-epa:20060008.

[18] T. C. Y. Wang et al. "Output filter design for a grid-interconnected three-phase inverter". In: *Proc. PESC '03. IEEE 34th Annual Conf. Power Electronics Specialist*. Vol. 2. June 2003, 779–784 vol.2. DOI: 10.1109/PESC.2003.1218154.

[19] Q. Zhao, F. Liang, and W. Li. "A new control scheme for LCL-type grid-connected inverter with a Notch filter". In: *Proc. 27th Chinese Control and Decision Conf. (2015 CCDC)*. May 2015, pp. 4073–4077. DOI: 10.1109/CCDC.2015.7162637.

[20] W. Zhao and G. Chen. "Comparison of active and passive damping methods for application in high power active power filter with LCL-filter". In: *Proc. Int. Conf. Sustainable Power Generation and Supply*. Apr. 2009, pp. 1–6. DOI: 10.1109/SUPERGEN.2009.5347992.